

Supporting Information

Enhanced photocatalytic H₂ evolution: Optimized atomic hydrogen desorption via free-electron transfer in sulfur-rich MoWS_{2+x} on vacancy-engineered CdS crystals

Ruiding Fei^{a,1}, Jianfeng Zhao^{b,1}, Huinan Wang^a, Huijuan Lin^a, Kui Xu^a, Guang Zeng^b,
Wenchao Wang^{c,d}, Zhiping Yan^{a,*}

^a School of Flexible Electronic (Future Technologies), Key Laboratory of Flexible Electronics (KLOFE), Nanjing Tech University, 30 South Puzhu Road, Nanjing 211816, P.R. China

^b State Key Laboratory of Catalysis, Dalian Institute of Chemical Physics, Chinese Academy of Sciences, Dalian 116023, P.R. China

^c School of New Energy, Nanjing University of Science & Technology, Jiangyin 214443, P.R. China

^d Department of Chemistry, The University of Hong Kong, Pokfulam Road. Hong Kong SAR, P.R. China

* Corresponding author' email address: iamzpyan@njtech.edu.cn (Z. Yan).

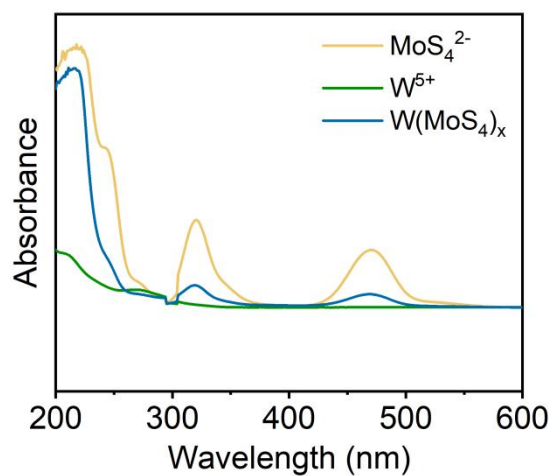
¹ Those authors contribute equally to this work.

Table of Contents

Figure S1. (a) UV-visible absorption spectrum of MoS_4^{2-} , W^{5+} and $\text{W}(\text{MoS}_4)_x$ solutions. (b) the corresponding photographs for the color change of CdS_v , $\text{W}^{5+}/\text{CdS}_v$, $\text{W}(\text{MoS}_4)_x/\text{CdS}_v$, and $\text{MoWS}_{2+x}/\text{CdS}_v$ suspensions.	4
Figure S2. SEM image of (a) CdS_v and (b) $\text{MoS}_{2+x}/\text{CdS}_v$	5
Figure S3. SEM image of (a) CdS , (b) $\text{MoS}_{2+x}/\text{CdS}$ and (c) $\text{MoWS}_{2+x}/\text{CdS}$	5
Figure S4. EPR spectra of CdS_v and MWC-3.	6
Figure S5. (a) XPS survey spectra of Cd 3d, S 2p, Mo 3d, W 4f and S 2s. (b) A magnified view of W 4f in the XPS survey spectrum.	7
Figure S6. Fourier transform infrared spectroscopy of MWC-3 and MWC-4.	8
Figure S7. Hydrogen evolution rates of CdS , $\text{MoS}_{2+x}/\text{CdS}$ and MWC-x' samples.	9
Figure S8. SEM images of MWC-3 (a) after 2 h irradiation ($\lambda \geq 420$ nm). (b) XRD patterns of MWC-3 before and after 2 h irradiation.	10
Figure S9. The raw data from absorption test of the NIR filter.	11
Figure S10. Photocurrent curves of CdS , $\text{MoS}_{2+x}/\text{CdS}$ and MWC-3'.	12
Figure S11. Mott-Schottky plots of (a) CdS_v and (b) $\text{MoS}_{2+x}/\text{CdS}_v$ in 0.5 M Na_2SO_4 tested at 1000 Hz, 2000 Hz and 3000 Hz, respectively.	13
Figure S12. Fs-TA measurements after 500 nm excitation with fluence of 2.2 uJ/pulse at visible region.	13
Figure S13. Density of states (DOS) diagram for (a) MoS_{2+x} and (b) MoWS_{2+x} (Illustrations for the respective computational models).	15
Table S1. Calculated quantum yields at different wavelengths.	16
Table S2. Composition (wt %) of the various samples based on the ICP-AES results.	16
Table S3. Comparison of H_2 evolution activity between molybdenum disulfide co-catalysts and cadmium sulfide based composite photocatalysts.	17
Table S4. The calculated carrier density of CdS_v , $\text{MoS}_{2+x}/\text{CdS}_v$, MWC-3 at 1000 Hz, 2000 Hz and 3000 Hz, respectively.	18

Table S5. Kinetic fitting parameters for MWC-3 at 1273 nm wavelengths after 410 nm excitation.....	18
Table S6. Kinetic fitting parameters for MWC-3 at 1273 nm wavelengths after 500 nm excitation.....	18
References	19

(a)



(b)

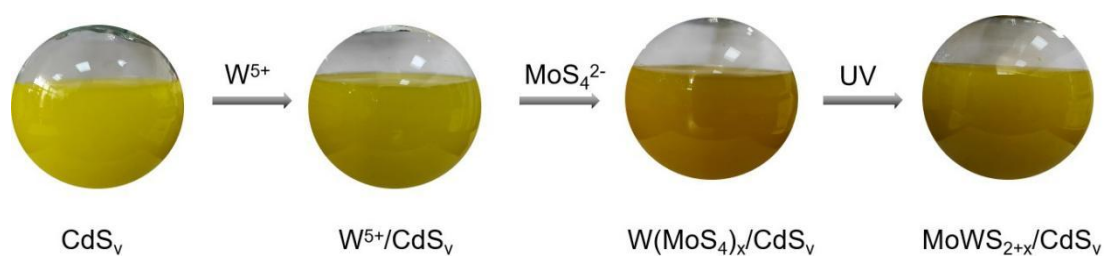


Figure S1. (a) UV-visible absorption spectrum of MoS_4^{2-} , W^{5+} and $\text{W}(\text{MoS}_4)_x$ solutions. (b) the corresponding photographs for the color change of CdS_v , $\text{W}^{5+}/\text{CdS}_v$, $\text{W}(\text{MoS}_4)_x/\text{CdS}_v$, and $\text{MoWS}_{2+x}/\text{CdS}_v$ suspensions.

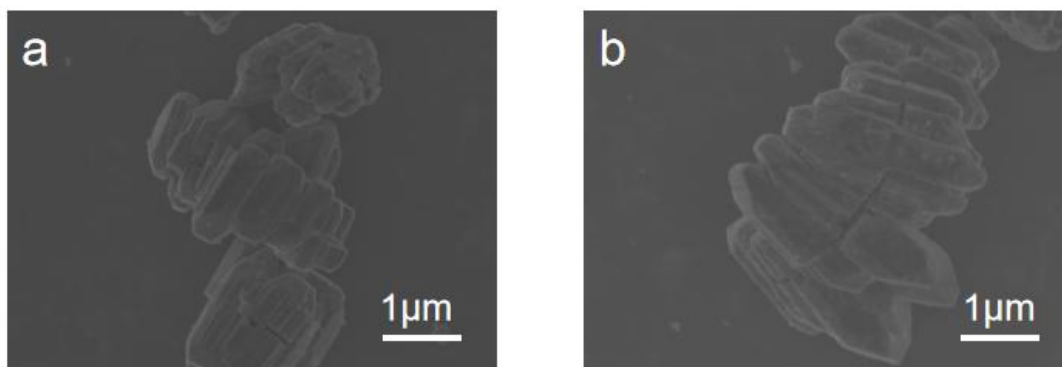


Figure S2. SEM image of (a) CdS_v and (b) MoS_{2+x}/CdS_v.

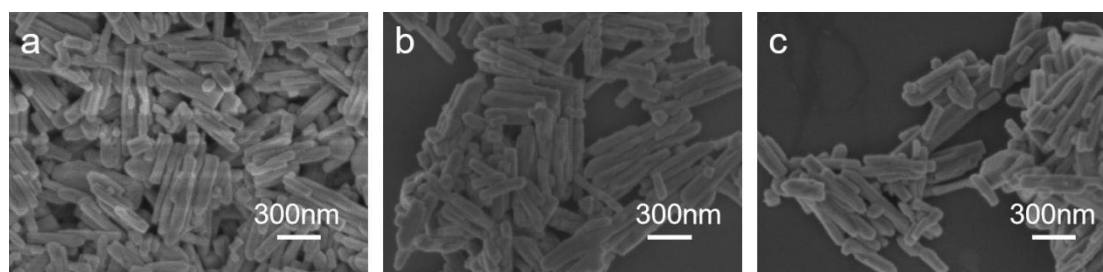


Figure S3. SEM image of (a) CdS, (b) MoS_{2+x}/CdS and (c) MoWS_{2+x}/CdS.

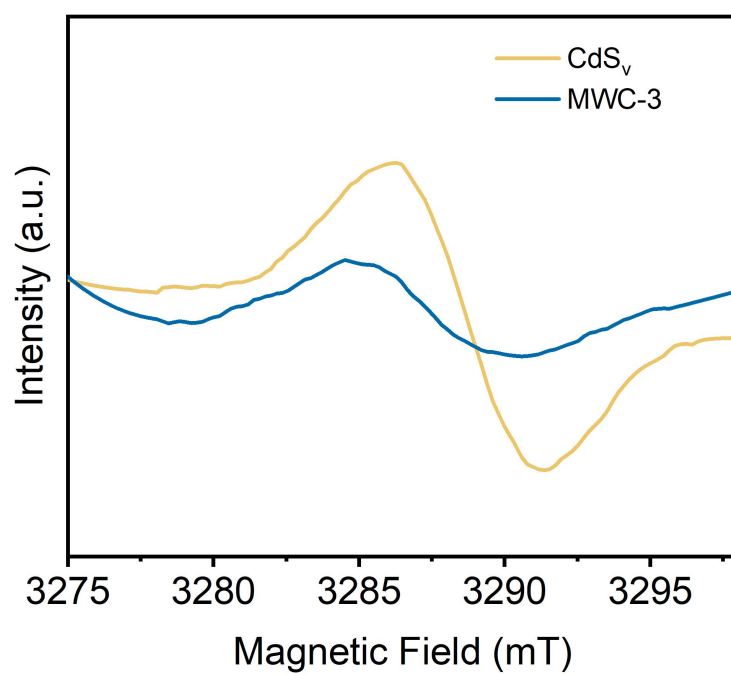


Figure S4. EPR spectra of CdS_v and MWC-3.

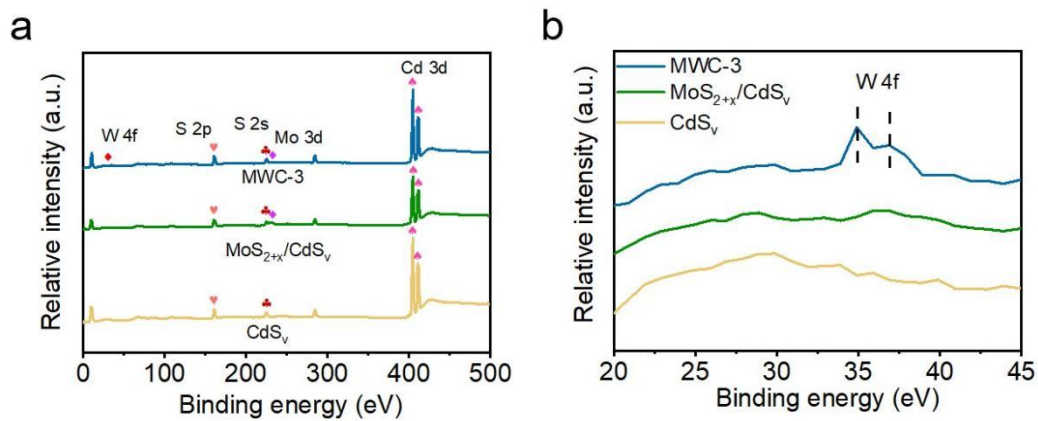


Figure S5. (a) XPS survey spectra of Cd 3d, S 2p, Mo 3d, W 4f and S 2s. (b) A magnified view of W 4f in the XPS survey spectrum.

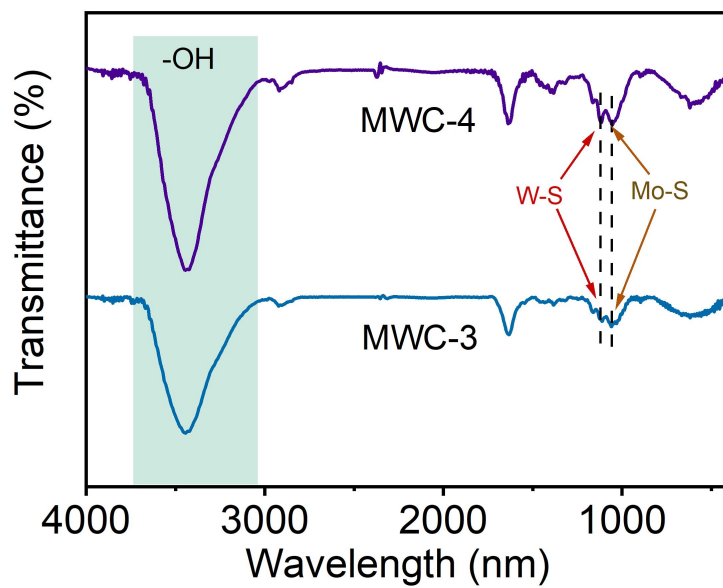


Figure S6. Fourier transform infrared spectroscopy of MWC-3 and MWC-4.

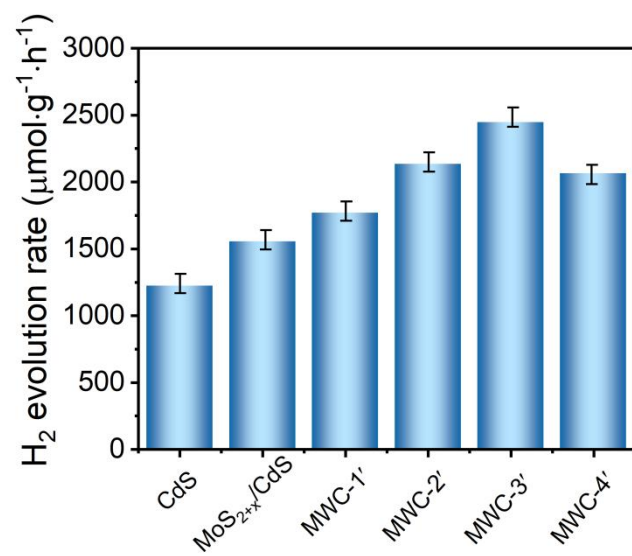


Figure S7. Hydrogen evolution rates of CdS, MoS_{2+x}/CdS and MWC-x' samples.

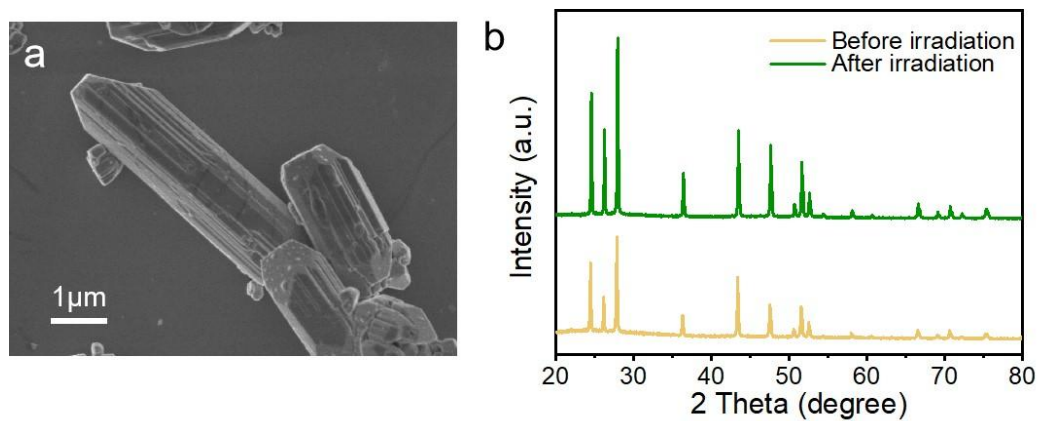


Figure S8. SEM images of MWC-3 (a) after 2 h irradiation ($\lambda \geq 420$ nm). (b) XRD patterns of MWC-3 before and after 2 h irradiation.

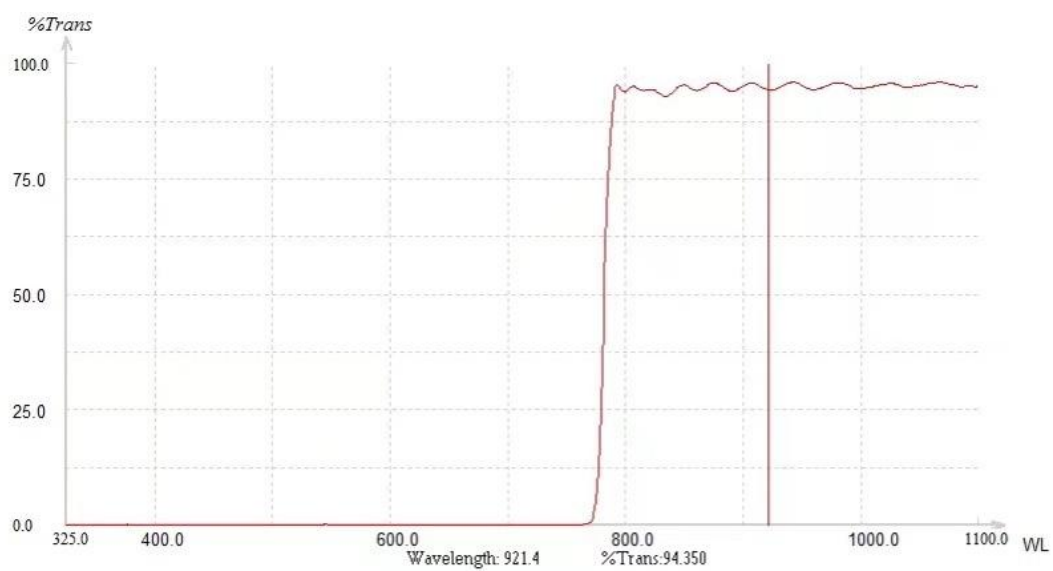


Figure S9. The raw data from absorption test of the NIR filter.

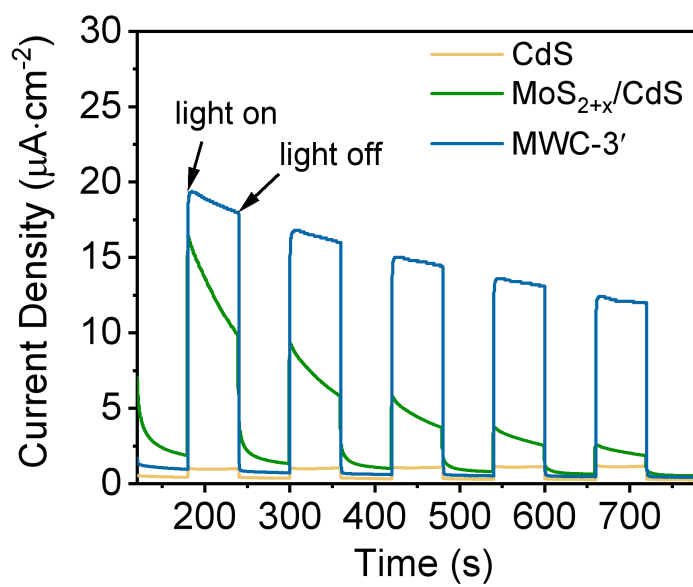


Figure S10. Photocurrent curves of CdS, MoS_{2+x}/CdS and MWC-3'.

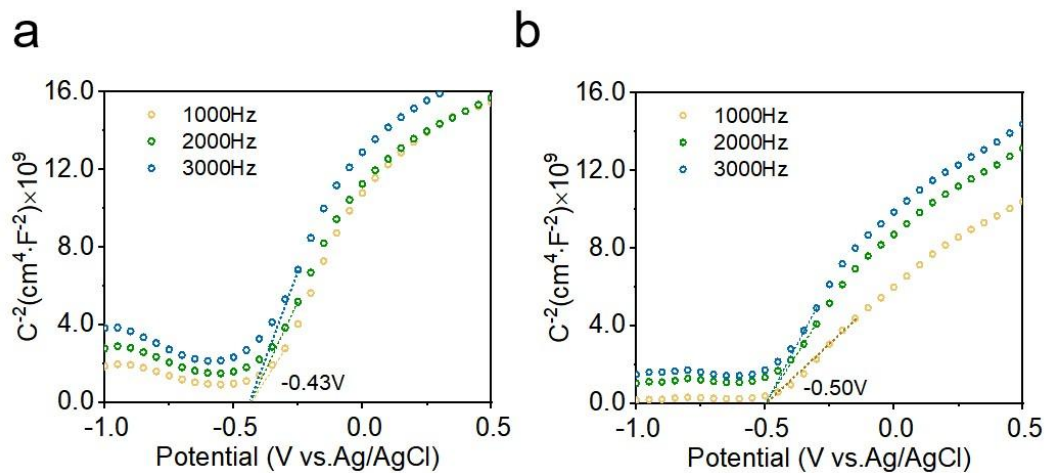


Figure S11. Mott-Schottky plots of (a) CdS_v and (b) $\text{MoS}_{2+x}/\text{CdS}_v$ in 0.5 M Na_2SO_4 tested at 1000 Hz, 2000 Hz and 3000 Hz, respectively.

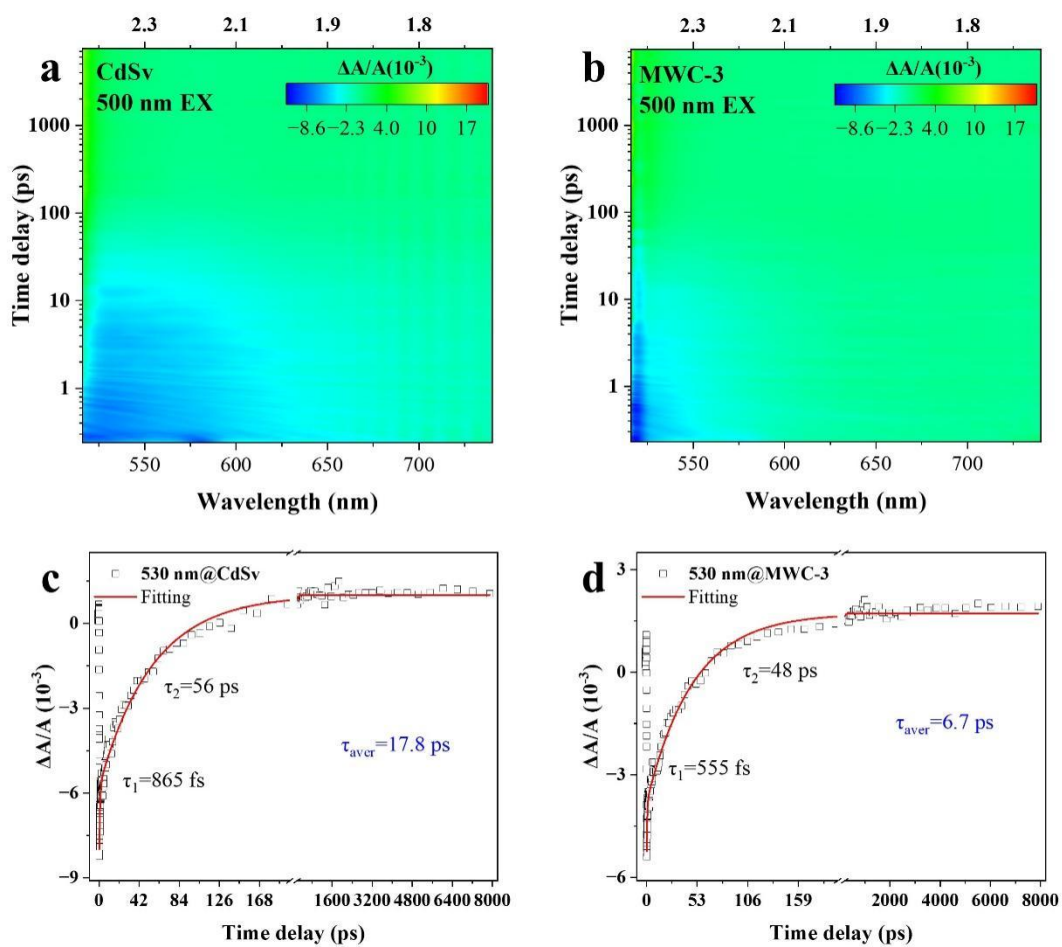


Fig. S12. Fs-TA measurements after 500 nm excitation with fluence of $2.2 \mu\text{J}/\text{pulse}$ at visible region: (a, b) The contour maps of samples upon 500 nm excitation, (c, d) the kinetic fitting at 530 nm for corresponding samples.

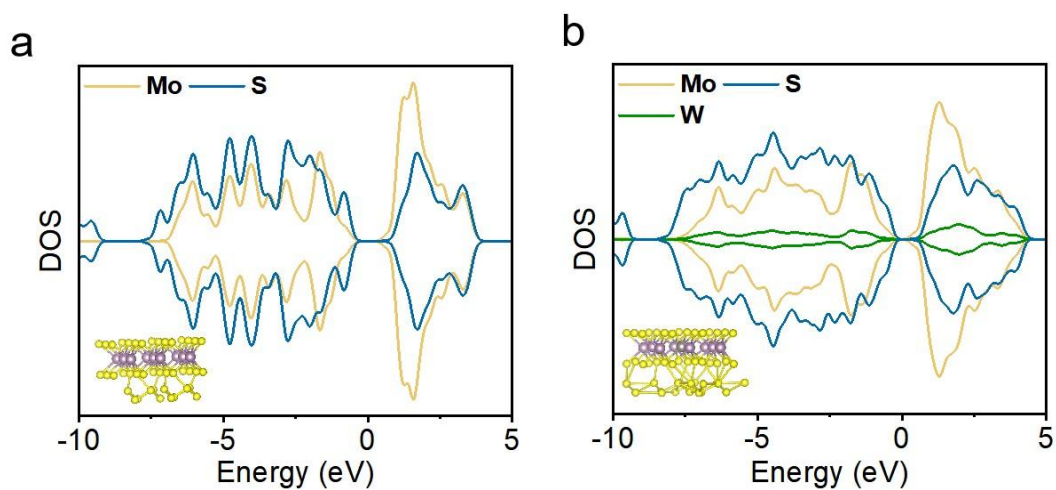


Figure S13. Density of states (DOS) diagram for (a) MoS_{2+x} and (b) MoWS_{2+x} (Illustrations for the respective computational models).

Table S1. Calculated quantum yields at different wavelengths.

λ (nm)	A (cm ²)	E (mW·cm ⁻²)	Chromatographic indication	R_{H_2} (μmol·h ⁻¹)	QE
390-400	2	12.5	1.6043	19.637	19.13%
420-430	2	19.8	2.0608	25.2238	14.40%
440-450	2	27.3	2.9018	35.5184	14.04%
480-485	2	16.2	1.8426	22.553	13.77%
500-510	2	13.2	1.1017	13.4848	9.70%

Table S2. Composition (wt %) of the various samples based on the ICP-AES results.

Samples	S (at.%)	Mo (at.%)	W (at.%)	S/(Mo+W)
MoWS _{2+x} /TiO ₂	8.64	0.019	0.039	> 2

Table S3. Comparison of H₂ evolution activity between molybdenum disulfide cocatalysts and cadmium sulfide based composite photocatalysts.

Photocatalysts	Light source	Incident light	Photocatalytic performance	AQY	Ref.
CdS/Mo-VC	300 W Xe light	$\lambda \geq 420$ nm	H ₂ rate: 2267 $\mu\text{mol} \cdot \text{g}^{-1} \cdot \text{h}^{-1}$	4.3% (420 nm)	[1]
MoWS _{2+x} /TiO ₂	4 LED light	$\lambda \geq 365$ nm	H ₂ rate: 4620.8 $\mu\text{mol} \cdot \text{g}^{-1} \cdot \text{h}^{-1}$	22.2% (365 nm)	[2]
TiO ₂ /Au@MoS _{2+x}	4 LED light	$\lambda \geq 365$ nm	H ₂ rate: 7858.1 $\mu\text{mol} \cdot \text{g}^{-1} \cdot \text{h}^{-1}$	38.1% (365 nm)	[3]
NiCd/CdS	300 W Xe light	$\lambda > 410$ nm	H ₂ rate: 11570 $\mu\text{mol} \cdot \text{g}^{-1} \cdot \text{h}^{-1}$	/	[4]
RuMoS _{2+x} /TiO ₂	4 LED light	$\lambda \geq 365$ nm	H ₂ rate: 2649.3 $\mu\text{mol} \cdot \text{g}^{-1} \cdot \text{h}^{-1}$	10.73% (365 nm)	[5]
ZnO/CdS/MoS ₂	300 W Xe light	$\lambda \geq 420$ nm	H ₂ rate: 10247.4 $\mu\text{mol} \cdot \text{g}^{-1} \cdot \text{h}^{-1}$	/	[6]
CdS-MoS ₂ -CoO _x	300 W Xe light	$\lambda \geq 420$ nm	H ₂ rate: 7400 $\mu\text{mol} \cdot \text{g}^{-1} \cdot \text{h}^{-1}$	7.6% (420nm)	[7]
MoSe ₂ /CdS	300 W Xe light	$\lambda \geq 420$ nm	H ₂ rate: 4700 $\mu\text{mol} \cdot \text{g}^{-1} \cdot \text{h}^{-1}$	15.6% (450 nm)	[8]
CdS/MoC	300 W Xe light	$\lambda \geq 420$ nm	H ₂ rate: 224.5 $\mu\text{mol} \cdot \text{g}^{-1} \cdot \text{h}^{-1}$	7.6% (420 nm)	[9]
MoWS _{2+x} /CdS _v	300 W Xe light	$\lambda \geq 420$ nm	H ₂ rate: 9166.13 $\mu\text{mol} \cdot \text{g}^{-1} \cdot \text{h}^{-1}$	19.13% (390 nm)	This work

Table S4. The calculated carrier density of CdS_v, MoS_{2+x}/CdS_v, MWC-3 at 1000 Hz, 2000 Hz and 3000 Hz, respectively.

Frequency	Carrier Density (cm ⁻³)		
	CdS _v	MoS _{2+x} /CdS _v	MWC-3
1000Hz	5.73×10 ²¹	7.63×10 ²¹	9.11×10 ²¹
2000Hz	4.28×10 ²¹	4.66×10 ²¹	6.73×10 ²¹
3000Hz	3.85×10 ²¹	4.13×10 ²¹	5.12×10 ²¹

Table S5. Kinetic fitting parameters for MWC-3 and CdS_v at 1273 nm upon 410 nm excitation.

Sample	λ (nm)	τ ₁ /ps	A ₁ (%)	τ ₂ /ps	A ₂ (%)	τ _{aver} /ps
MWC-3	1273	12.1	86.2	77.6	13.8	21.2
CdS _v	1273	10.1	59.7	104.5	40.3	48.2

Table S6. Kinetic fitting parameters for MWC-3 and CdS_v at 1273 nm wavelengths upon 500 nm excitation.

Sample	λ (nm)	τ ₁ /ps	A ₁ (%)	τ ₂ /ps	A ₂ (%)	τ _{aver} /ps
MWC-3	1273	4.1	59.5	106	40.5	45.4
CdS _v	1273	NA	NA	NA	NA	NA*

Note: NA* means that there is no absorption peak at 1273 nm for the corresponding sample, so it is not applicable (NA).

References

- [1] Y. Lei, K.H. Ng, Y. Zhu, Y. Zhang, Z. Li, S. Xu, J. Huang, J. Hu, Z. Chen, W. Cai, Y. Lai, *Chem. Eng. J.*, 452 (2023) 139325.
- [2] D. Gao, B. Zhao, L. Wang, E. Aslan, I. Hatay Patir, J. Yu, H. Yu, *Chem. Eng. J.*, 449 (2022) 137803.
- [3] D. Gao, P. Deng, J. Zhang, L. Zhang, X. Wang, H. Yu, J. Yu, *Angew. Chem., Int. Ed.*, 62 (2023) e202304559.
- [4] B. Wang, S. He, L. Zhang, X. Huang, F. Gao, W. Feng, P. Liu, *Appl. Catal. B: Environ.*, 243 (2019) 229-235.
- [5] W. Zhong, D. Gao, P. Wang, X. Wang, H. Yu, *Appl. Catal. B: Environ.*, 319 (2022) 121910.
- [6] Y. Jia, Z. Wang, X.-Q. Qiao, L. Huang, S. Gan, D. Hou, J. Zhao, C. Sun, D.-S. Li, *Chem. Eng. J.*, 424 (2021) 130368.
- [7] T. Di, Q. Deng, G. Wang, S. Wang, L. Wang, Y. Ma, *J. Mater. Sci. Technol.*, 124 (2022) 209-216.
- [8] X. Yang, W. Liu, C. Han, C. Zhao, H. Tang, Q. Liu, J. Xu, *Mater. Today Phys.*, 15 (2020) 100261.
- [9] Y. Lei, X. Wu, S. Li, J. Huang, K.H. Ng, Y. Lai, *J. Cleaner Prod.*, 322 (2021) 129018.